energies

Article

A Variable-Weather-Parameter MPPT Method Based on Equation Solution for Photovoltaic System with DC Bus

Shaowu Li *, Kunyi Chen, Qin Li and Qing Ai

College of Intelligent Systems Science and Engineering, Hubei Minzu University, Enshi 445000, China
* Correspondence: xidu_surfer@163.com; Tel.: +86-139-9779-9701

Abstract: The control signals of the variable-weather-parameter (VWP) methods need to be calculated by the real-time measured data of the irradiance and temperature (I&T) sensors, which leads to the high hardware cost of the sensors. To solve this problem, the PV system with a DC bus is selected as the research subject and a novel maximum power point tracking (MPPT) method is proposed. It is named the VWP MPPT method based on the equation solution (ES-VWP method). Its control signal is directly calculated by the solution of an established equation set rather than data measured by the I&T sensors. This equation set consists of two integrated mathematical equations, which represent two different operating points of the PV system. Meanwhile, when the bus voltage is varying or unknown, a calculation method that can estimate the real-time value of the DC bus voltage is proposed. In addition, an implementation method corresponding to the ES-VWP method is also designed. Finally, some simulation experiments are carried out to verify the availability and feasibility of the ES-VWP method. Meanwhile, some simulation experiments show that the error of the equation solution is less than 0.0001. In addition, some simulation experiments illustrate that the MPPT settling times of the ES-VWP method are always less than one-tenth of the P&O method (or one-sixth of the FLC method). Compared with the existing VWP methods, it can be implemented without the use of I&T sensors or external I&T data. Meanwhile, compared with other existing MPPT methods, its better MPPT rapidity originating from the advantage of the VWP methods is inherited. This work is the first attempt to design a novel MPPT method by obtaining the real-time equation solutions of V_{oc} and I_{sc}. Meanwhile, this work is also the first attempt to solve the real-time equation of V_{bus} by the solved V_{oc} and I_{sc}. In addition, this work is also the first attempt to design an implementation method for establishing an equation set by sampling two operating points of a PV system at the same time.

Keywords: PV system; MPPT; equation solution; VWP method; MPP

Citation: Li, S.; Chen, K.; Li, Q.; Ai, Q. A Variable-Weather-Parameter MPPT Method Based on Equation Solution for Photovoltaic System with DC Bus. *Energies* **2022**, *15*, 6671. https://doi.org/10.3390/en15186671

Academic Editor: Carlo Renno

Received: 1 August 2022
Accepted: 9 September 2022
Published: 13 September 2022

1. Introduction

Up to now, a lot of MPPT methods have been proposed [1,2]. They mainly include some conventional methods (such as the P&O method [3], INC method [4], etc.), some intelligent methods (such as the FLC method [5], SSO method [6], etc.), and other methods (such as the VWP methods [7,8], SCC method [9], etc.). Meanwhile, some studies on the mathematical equations of the PV system have also been presented. For example, a Monod equation was presented to estimate the output power and then an MPPT method was proposed [10]. Moreover, the $V-I$ characteristic implicit equation of the PV cell was applied to analyze the relationships between some parameters solved by an optimization algorithm [11]. In addition, some integrated equations have been proposed to analyze the $V-I$ characteristics of the PV system [12]. As everyone knows, these implicit equations or integrated equations implicate the regularity of the MPP varying with irradiance and temperature. However, hitherto, it is very difficult to directly use them to design the new MPPT method of the PV system. The primary reason is the lack of a direct relationship between them and the MPP control signal, especially under fast varying irradiance and temperature conditions. To sweep away this obstacle, in this work, the relationship between the $V - I$ characteristics and MPP control signal is identified by solving a built integrated equation of the PV system. On the basis of this, a novel MPPT method is designed and proposed. In this work, the regularity with which the MPP varies with irradiance and temperature is disclosed by the equation solution, which is beneficial to improving the understanding level of the MPPT control law based on the integrated equations of the PV system.

In existing MPPT methods, the VWP methods have the fastest MPPT speed [7,8]. However, they suffer from the high cost of the I&T sensors. Therefore, when they are thoroughly studied, one of the main tasks is to find the perfect balance between low hardware costs and a good MPPT performance. Clearly, an effective way is the abandonment of the irradiance or temperature sensors, and now some attempts have been made. For example, without an irradiance sensor, a short-circuit current MPPT method was presented to improve the MPPT capability of the conventional P&O method [13]. However, here, the real-time value of the short-circuit current must be measured, so the system complexity and MPPT performance are greatly influenced. Meanwhile, to reduce the hardware cost arising from I&T sensors, the weather forecast data has been used to design a VWP method [14]. However, the usage of the external forecast data implies extra equipment and a worrying accuracy. Obviously, some serious shortcomings have appeared after the I&T sensors were thrown away. To solve this difficult problem, in this work, a direct calculation method of the real-time control signal is proposed by solving an equation set. Here, this established equation set consists of two integrated equations of the PV system with a DC bus. The aim of the equation solution is to obtain the real-time values of V_{oc} and I_{sc} after the output voltage and current are measured. Clearly, the design of this MPPT control process is very different from all existing VWP methods or other MPPT methods. The main difference arises from a transformation, in that the real-time data of the I&T sensors is replaced by the solved V_{oc} and I_{sc}. Meanwhile, this transformation also reveals the lower hardware cost and better control independence because no extra sensor or external data is needed in the MPPT achievement.

In addition, some MPPT methods are aimed at PV systems with a battery output and DC bus output. When batteries are used as the output of the PV system, its output voltage can be regarded as a constant. For example, a global MPPT method is proposed by scanning the characteristics of the batteries to overcome some shortcomings of the existing MPPT methods [15]. A sliding mode MPPT method was proposed when a battery bank was connected with the DC/DC converter of a PV system [16]. An MPPT method based on an introduced complex function was presented for a PV system with a battery output [17]. In contrast, there are some works on a PV system with a DC bus. For example, an efficiency comparison of the AC and DC power network was presented by simulation [18]. A global MPPT method based on PSO was proposed for the distributed PV system with a DC bus [19]. Meanwhile, an MPPT method based on robust input-output linear control was presented for a PV system with a DC bus [20]. Obviously, these PV systems can be unified and regarded as PV systems with a DC bus. Usually, the bus voltage is constant and is represented by V_{bus}. However, in practical applications, V_{bus} may vary in a large or small range, which will lead to inaccuracy in the calculated control signal. If a measurement circuit or sensor is used to measure its real-time value, the hardware cost is increased. To deal with this issue, in this work, a numerical solution method of V_{bus} is proposed. In this work, on the one hand, the gap in solving the real-time value of V_{bus} based on an established equation is filled in. On the other hand, the relationship between the operating point and V_{bus}, especially under varying DC bus conditions, is disclosed.

The main contributions and innovations of this work can be illustrated as follows:

(1) A novel MPPT method is proposed by obtaining the real-time equation solutions of V_{oc} and I_{sc}. Meanwhile, it is unnecessary to solve the established equation set of the PV system with a DC bus at the MPP. Therefore, this MPPT method is very different from all existing VWP methods or other MPPT methods.

(2) The real-time value of V_{bus} is first solved successfully by the obtained values of V_{oc} and I_{sc}. This work not only fills in the gap in obtaining the real-time equation solution of V_{bus} but also discloses the relationship between the bus voltage and other circuit parameters.
(3) An implementation method for the ES-VWP method is successfully designed. This work is the first attempt to establish an equation set by sampling two operating points of a PV system at the same time.
(4) In this work, the external data or measured values of the irradiance and temperature are no longer needed when an existing VWP method is implemented. Therefore, the lower hardware cost and better control independence can be achieved, which is beneficial to the widespread use of the VWP methods.

This work is arranged as follows: the principle of the ES-VWP method is analyzed in Section 2. This MPPT method is proposed and described in Section 3. Meanwhile, its implementation circuit and control process are designed in Section 4. The accuracy, feasibility, and availability of the ES-VWP method are verified, and the MPPT steady-state and transient-state performances are analyzed in Section 5. Finally, some conclusions are drawn in Section 6.

2. Principle

2.1. Mathematical Modeling of the PV System with a DC Bus

The PV system with a DC bus is shown in Figure 1. In this paper, the buck DC/DC converter (or buck circuit) is used as the MPPT circuit. By analogy, other converters can also be analyzed.

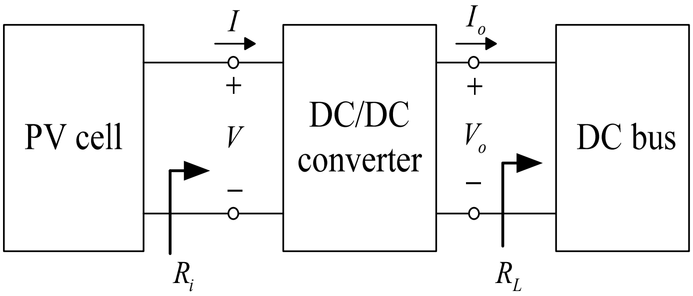

Figure 1. Structure of the common PV system with a DC bus.

For the PV cell, its mathematical model is shown in Equations (1)–(3) [21,22]. It is usually called the four-parameter model in engineering applications [22]:

$$I = I_{sc}[1 - C_1(e^{\frac{V}{C_2 V_{oc}}} - 1)] \quad (1)$$

$$C_1 = \left[1 - \frac{I_m}{I_{sc}}\right] e^{-\frac{V_m}{C_2 V_{oc}}} \quad (2)$$

$$C_2 = \frac{\frac{V_m}{V_{oc}} - 1}{\ln\left[1 - \frac{I_m}{I_{sc}}\right]} \quad (3)$$

For the buck circuit, its model is represented by Equation (4) [23]. Meanwhile, its input power (P_i) and output power (P_o) are represented by Equations (5) and (6), respectively:

$$V_o = DV \quad (4)$$

$$P_i = VI \quad (5)$$

$$P_o = V_o I_o \quad (6)$$

For the DC bus, its model is represented by Equation (7):

$$V_o = V_{bus} \tag{7}$$

Assume that, under ideal conditions, there is no power loss to the DC/DC converter, therefore, Equation (8) can be satisfied:

$$P_o = P_i \tag{8}$$

According to Equations (1) and (4)–(8), Equation (9) is satisfied under ideal conditions:

$$P_o = P_i = \frac{V_{bus} I_{sc}}{D}\left[1 - C_1(\mathrm{e}^{\frac{V_{bus}}{C_2 D V_{oc}}} - 1)\right] \tag{9}$$

Equation (9) is the integrated equation of the PV system with a DC bus under ideal conditions when the buck circuit is used. It can be used to establish the equation set, which is the theoretical basis of the new proposed VWP method.

2.2. Establishment of the Equation Set

According to our previous work in [24], the control signal at the MPP can be calculated by Equation (10) for the PV system with a DC bus:

$$D_{\max} = \frac{V_{bus}}{C} \tag{10}$$

where:

$$C = C_2 V_{oc}[\text{lambertw}(\mathrm{e} \times \frac{1 + C_1}{C_1}) - 1] \tag{11}$$

Equation (11) can be replaced by Equation (12):

$$C = C_C V_{oc} \tag{12}$$

where $C_C = C_2[\text{lambertw}(\mathrm{e} + \mathrm{e}/C_1) - 1]$. Here, we can assume that C_C is a constant, and then Equation (13) is satisfied:

$$D_{\max} = \frac{V_{bus}}{C_C V_{oc}} \tag{13}$$

Obviously, according to Equation (13), the calculated value of $D_{\max}$ is determined by the three parameters (V_{bus}, C_C, and V_{oc}). Meanwhile, the bus voltage of the PV system is usually constant, so V_{bus} can be regarded as a known parameter. In this case, it is of importance to obtain the real-time value of V_{oc}.

Therefore, two different operating points A (V_1, I_1, D_1) and B (V_2, I_2, D_2) are first selected, and then, Equations (14) and (15) are given by submitting them into Equation (9), respectively:

$$P_{o1} = P_{i1} = \frac{V_{bus} I_{sc}}{D_1}\left[1 - C_1(\mathrm{e}^{\frac{V_{bus}}{C_2 D_1 V_{oc}}} - 1)\right] \tag{14}$$

$$P_{o2} = P_{i2} = \frac{V_{bus} I_{sc}}{D_2}\left[1 - C_1(\mathrm{e}^{\frac{V_{bus}}{C_2 D_2 V_{oc}}} - 1)\right] \tag{15}$$

By submitting Equation (5) into Equations (14) and (15), then Equations (16) and (17) are satisfied, respectively:

$$V_1 I_1 = \frac{V_{bus} I_{sc}}{D_1}\left[1 - C_1(\mathrm{e}^{\frac{V_{bus}}{C_2 D_1 V_{oc}}} - 1)\right] \tag{16}$$

$$V_2 I_2 = \frac{V_{bus} I_{sc}}{D_2}\left[1 - C_1(\mathrm{e}^{\frac{V_{bus}}{C_2 D_2 V_{oc}}} - 1)\right] \tag{17}$$

When two operating points A and B are different from each other, Equations (16) and (17) are two independent equations. Therefore, an equation set can be established by combining them, and Equation (18) can be presented:

$$\begin{cases} V_1 I_1 = \frac{V_{bus} I_{sc}}{D_1}\left[1 - C_1(e^{\frac{V_{bus}}{C_2 D_1 V_{oc}}} - 1)\right] \\ V_2 I_2 = \frac{V_{bus} I_{sc}}{D_2}\left[1 - C_1(e^{\frac{V_{bus}}{C_2 D_2 V_{oc}}} - 1)\right] \end{cases} \quad (18)$$

Meanwhile, to simplify Equation (18), Equations (4) and (7) are submitted into it. Then, Equation (19) can be given:

$$\begin{cases} I_{sc}[1 - C_1(e^{\frac{V_1}{C_2 V_{oc}}} - 1)]|_{D_1} = I_1 \\ I_{sc}[1 - C_1(e^{\frac{V_2}{C_2 V_{oc}}} - 1)]|_{D_2} = I_2 \end{cases} \quad (19)$$

According to our previous work in [25], C_1 and C_2 can be assumed as two constants. Therefore, only two unknown numbers (I_{sc} and V_{oc}) exist in Equation (19) when the real-time V (V_1 or V_2) and I (I_1 or I_2) are obtained by the measurement circuits (or sensors).

Obviously, after the real-time values of these two parameters (I_{sc} and V_{oc}) have been solved by Equation (19), the control signal at the MPP can be successfully calculated by Equation (10) in real time. This is the principle of proposing and designing the new MPPT method.

2.3. Equation Solution of the Bus Voltage

Generally, the bus voltage of the PV system is given or remains constant. In this case, its value can be easily obtained. However, in practical applications, it may vary in a large or small range. If it varies or its value is unknown, V_{bus} can still be obtained by the equation solution.

According to Equation (17), Equation (20) can be given as:

$$V_{bus} = \frac{D_2 V_2 I_2}{I_{sc}\left[1 - C_1\left(e^{\frac{V_{bus}}{C_2 D_2 V_{oc}}} - 1\right)\right]} \quad (20)$$

Clearly, V_{bus} can be calculated after V_2 and I_2 have been measured. Here, I_{sc} and V_{oc} are solved by Equation (19), and D_2 is directly read by the controller. Therefore, Equation (20) is the theory basis for solving the real-time value of the DC bus voltage.

In addition, theoretically, the real-time value of V_{bus} can also be solved by Equation (21). This equation is built by the operating point A.

$$V_{bus} = \frac{D_1 V_1 I_1}{I_{sc}\left[1 - C_1\left(e^{\frac{V_{bus}}{C_2 D_1 V_{oc}}} - 1\right)\right]} \quad (21)$$

However, in this work, Equation (20) is used to solve the real-time value of V_{bus} rather than Equation (21). Two main reasons can be illustrated as follows: on the one hand, this choice is determined by the designs of the system configuration and the MPPT control process. They are presented and introduced in Section 4. On the other hand, the accuracy of the equation solution is considered. This issue is analyzed in Sections 4.2 and 5.1.3.

3. Proposition

According to Equation (13), a new VWP method can be proposed and described: for the MPPT controller of the PV system with a DC bus, its real-time MPP control signal ($D_{\max}$) can be directly calculated by Equation (13) after V_{oc} is solved by Equation (19) in real time. If V_{bus} varies or is unknown, the real-time value of V_{bus} should also be solved by Equation (20) and then participate in the calculation of $D_{\max}$. In Equation (19), the points A (V_1, I_1, D_1) and B (V_2, I_2, D_2) are updated by the real-time measured values. Meanwhile, these two points must remain different from each other to make Equation (19) reasonable and available. Because the equation solution plays a key role in the real-time calculation of $D_{\max}$, this method is named the VWP MPPT method based on the equation solution (ES-VWP method).

Clearly, by comparing this ES-VWP method with other VWP methods, some characteristics can be shown: on the one hand, the good MPPT speed can be inherited by the direct calculation of $D_{\max}$, especially under varying weather conditions. On the other hand, in this ES-VWP method, the irradiance and temperature sensors (or external data of the I&T) are not needed, which means greatly reduced hardware costs. Therefore, this method is very different from other VWP methods.

4. Implementation

4.1. Design of System Configuration

A PV system corresponding to this proposed ES-VWP method is designed. Its configuration is shown in Figure 2. Generally, this PV system with a DC bus consists of PV subsystems 1-n, DC bus, DC loads, inverter with AC loads (grid or AC bus), bidirectional DC/DC converter with batteries, etc., as shown in Figure 2. Here, all PV subsystems are connected by a DC bus and an MPPT controller can be used to control them. In practical applications, the inverter, bidirectional DC/DC converter with batteries, and other units can also be controlled by this controller. However, in this work, only the MPPT control process is taken into account.

Figure 2 shows that, to obtain the points A (V_1, I_1, D_1) and B (V_2, I_2, D_2), the real-time values of V_1, I_1, V_2, and I_2 must be measured and sent into the MPPT controller. Here, these four parameters must be sampled at the same time. Three main reasons can be illustrated as follows: firstly, the synchronous sampling ensures the same weather conditions because I_{sc} and V_{oc} change with the varying weather. Therefore, the reasonableness and uniqueness of these two parameters can be ensured by the synchronously measured data. Secondly, in practical applications, some sampling error may be caused by the differences in the hardware, software, delay, inertia, etc. Therefore, to a certain extent, the synchronous sampling can reduce the error to ensure the accuracy. Thirdly, the good MPPT rapidity of the proposed method is ensured by the design (Figure 2) for synchronous sampling. In contrast, if two points A and B are sampled at regular intervals, it is difficult for the delay between two sampling intervals to be accepted because the MPPT rapidity will be greatly influenced by this delay.

Therefore, in this design, V_1 and I_1 are measured in PV subsystem 1 while V_2 and I_2 are measured in PV subsystem 2. Meanwhile, to make the points A and B different from each other all the time, the control signal of the buck DC/DC converter 1 is set as $D_{\max}$ while the buck DC/DC converter 2 is set as $D_{\max} - \Delta D$. Here, ΔD represents the duty cycle increment and is a small positive number. In this work, it is selected as 0.001. Meanwhile, the control signals of other PV subsystems (PV subsystems 3-n) are set as $D_{\max}$. In this case, only PV subsystem 2 is operating around MPP while other PV subsystems (including PV subsystem 1, PV subsystem 3, PV subsystem 4 . . . , PV subsystem n) are operating at the MPP. In addition, when V_{bus} must be solved by Equation (20), the control signal of the buck DC/DC converter 2 should be set as a default value (usually 1) rather than $D_{\max} - \Delta D$. This issue will be discussed in Section 4.2.

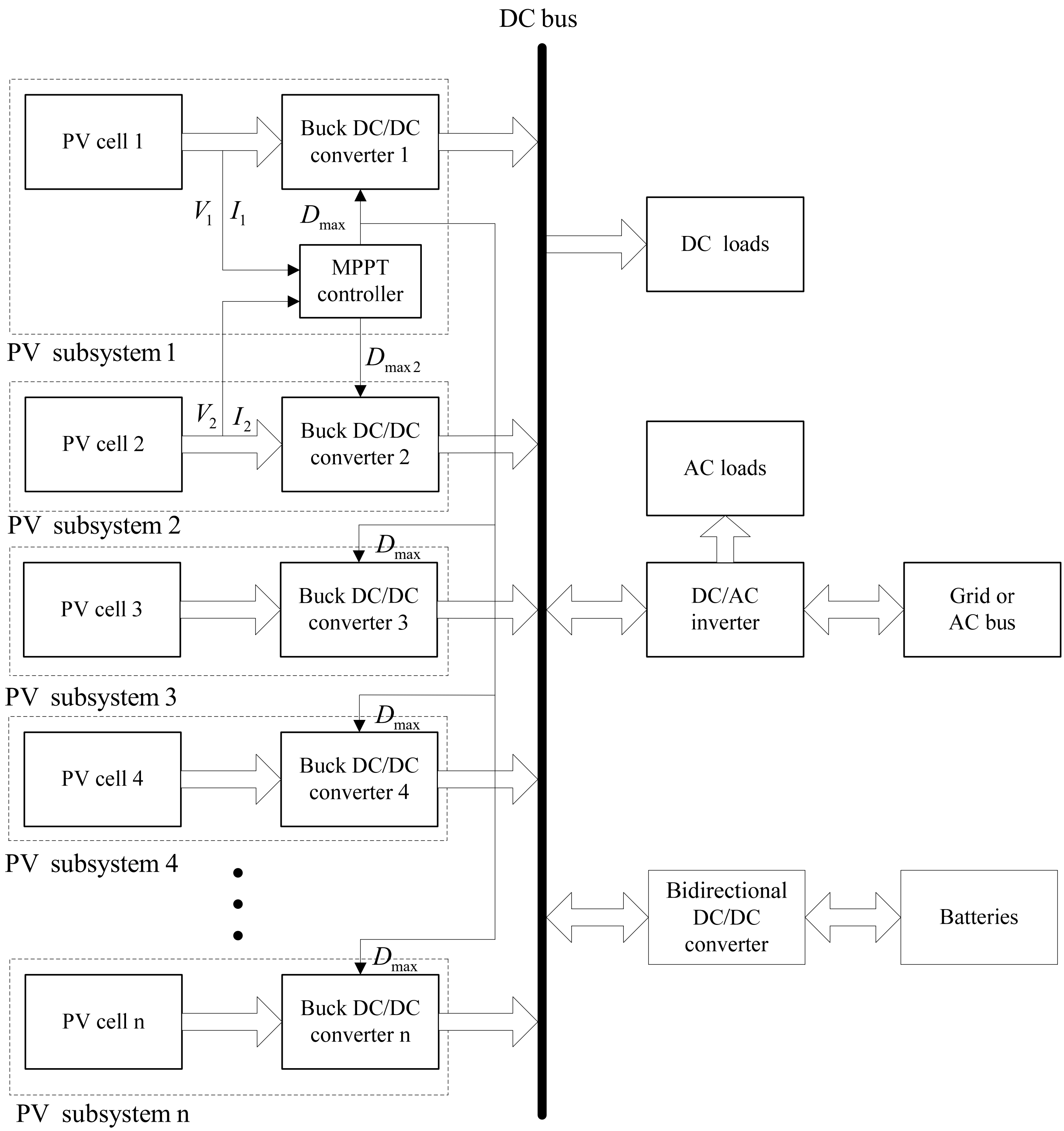

Figure 2. Designed system configuration for the ES-VWP method.

4.2. Design of the MPPT Control Process

After the system configuration is designed, as presented in Figure 2, the corresponding control process is also designed and is shown in Figure 3.

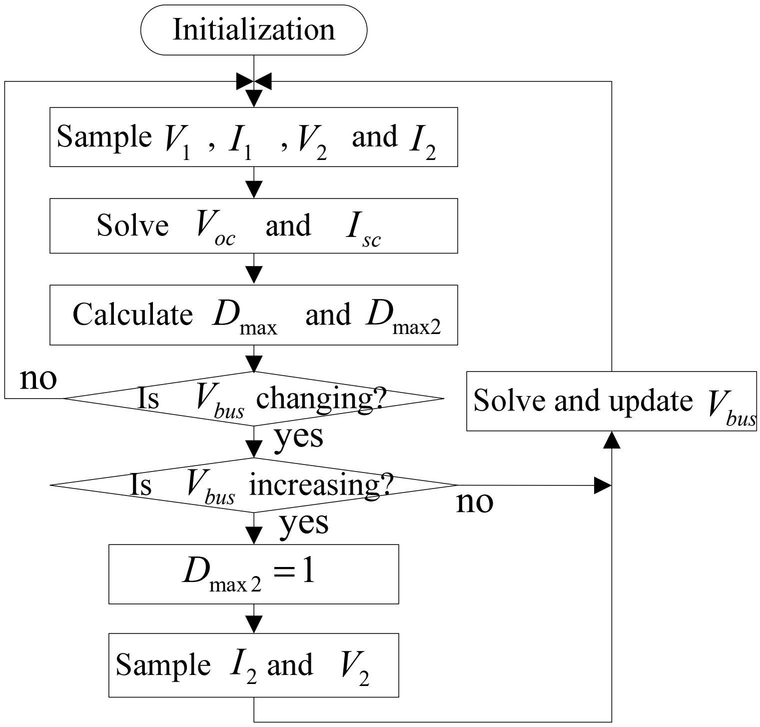

Figure 3. Designed MPPT control process.

Some initial tasks are finished in the step "Initialization". In the step "Sample V_1, I_1, V_2, and I_2", the real-time values of V_1, I_1, V_2, and I_2 are sampled by the measurement units and their mean values are obtained. Meanwhile, the real-time values of D_1 and D_2 are read by the MPPT controller. In the step "Solve V_{oc} and I_{sc}", V_{oc} and I_{sc} are solved by Equation (19). In the step "Calculate $D_{\max}$ and $D_{\max2}$", $D_{\max}$ and $D_{\max2}$ are calculated by Equations (13) and (22), respectively. If V_{bus} is unknown or varies, $D_{\max2}$ should be first set as 1 (a default value), and then V_2 and I_2 are sampled to obtain point B. Finally, in the step "Solve and update V_{bus}", V_{bus} is solved by Equation (20). Here, $D_{\max2}$ may not be set as 1, but its value must be bigger than the duty cycle at the MPP to ensure the accuracy of the solution. In addition, Equation (22) cannot be used when V_{bus} is being solved by the steps "Sample I_2 and V_2" and "Solve and update V_{bus}":

$$D_{\max2} = D_{\max} - \Delta D \tag{22}$$

According to Figures 2 and 3, obviously, there are some main advantages as follows: on the one hand, only some simple judgement, assignment, and calculation steps are needed if V_{bus} is constant and given. In this case, the control program is very simple, and its running speed is very fast, which results in a low-cost microprocessor, easy implementation, and short-period design (including hardware and software designs). If V_{bus} varies and is unknown, only before its value is solved, the running speed of the program is influenced to a certain degree. On the other hand, the MPPT speed, in addition to other VWP methods, is very fast because of the directly calculated control signal. Finally, by comparing the ES-VWP method with other VWP methods, the hardware cost is greatly reduced because not only the irradiance and temperature sensors but also any external irradiance and temperature data are not needed.

5. Simulation Analysis

After the ES-VWP method and its implementation were proposed, some simulations were carried out using the MATLAB/Simulink tool [26] to analyze the feasibility, availability, and accuracy of the equation solution; verify the feasibility and availability of the proposed method; and test the MPPT performance of the proposed method. In these simulations, the PV system shown in Figure 2 was built and the control process shown in Figure 3 was implemented. Meanwhile, a PV cell, whose four parameters I_{sc}, V_{oc}, I_m, and V_m are 9.19A, 22V, 8.58A, and 17.5V at STC, respectively, was selected in this work. If other PV cells whose parameters are different from this work are selected, the same (or similar) results can still easily be obtained by analogy.

5.1. Feasibility and Availability of the Equation Solution

5.1.1. Verification and Acquisition of C_C

To verify that C_C can be regarded as a constant and obtain its value, two simulation experiments were carried out. The results are shown in Figures 4 and 5. Here, the $C_C - S$ curve is given under 25 °C and varying irradiance conditions. Meanwhile, the $C_C - T$ curve is given under 1000 W/m^2 and varying temperature conditions.

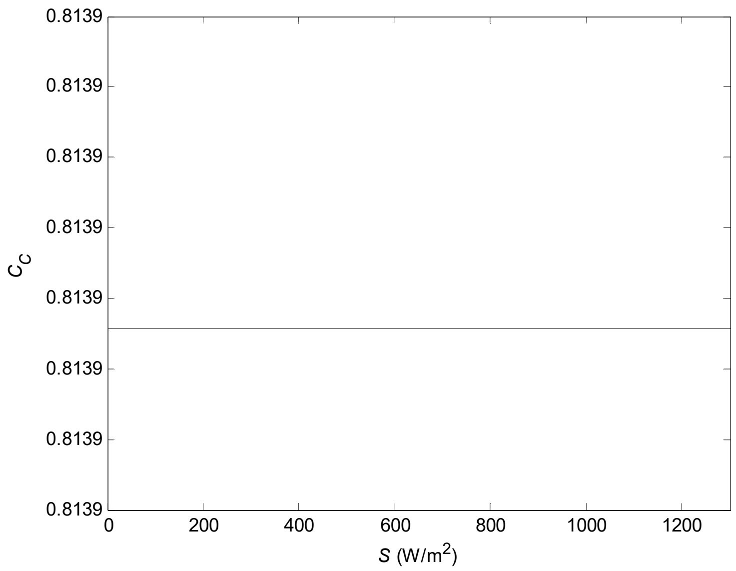

Figure 4. $C_C - S$ curve under the 25 °C condition.

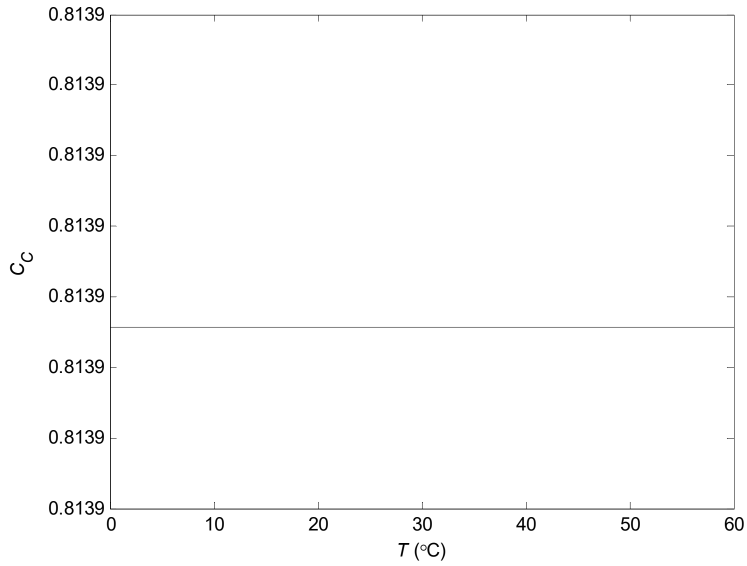

Figure 5. $C_C - T$ curve under the 1000 W/m^2 condition.

Figure 4 shows that C_C does not change under varying irradiance conditions. Meanwhile, Figure 5 shows that C_C does not change under varying temperature conditions. Therefore, in practical applications, it is reasonable that C_C is regarded as constant. In addition, according to Figures 4 and 5, the value of C_C is about 0.8139. Here, if other PV cells whose parameters are different from this work are selected, the corresponding value of C_C can still easily be obtained by analogy.

5.1.2. Verification of Equation (19)

To test whether I_{sc} and V_{oc} can be successfully solved by Equation (19), some simulation experiments were carried out. Figure 6 shows the simulation results under 1000 W/m^2, 20 °C, and different D conditions, and Figure 7 shows the simulation results under 800 W/m^2, 10 °C, and different D conditions. Here, the results under other weather conditions can be obtained by analogy.

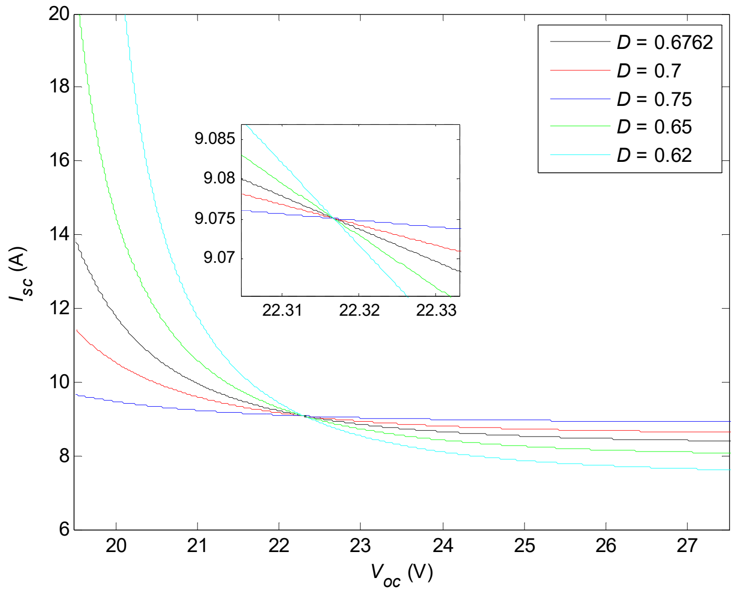

Figure 6. $I_{sc} - V_{oc}$ curves under 1000 W/m^2 and 25 °C conditions.

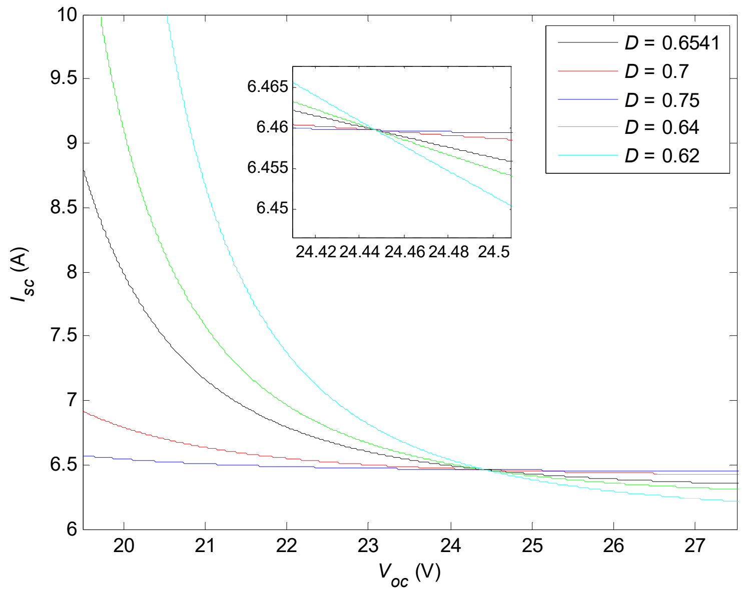

Figure 7. $I_{sc} - V_{oc}$ curves under 800 W/m^2 and 10 °C conditions.

Figures 6 and 7 show that, firstly, under a given weather condition, I_{sc} and V_{oc} can be successfully solved by Equation (19). Secondly, the uniqueness of the equation solution can be verified under a certain weather condition. Thirdly, this unique solution varies with the varying weather conditions. Therefore, a conclusion can be drawn that the real-time values of two cell parameters (I_{sc} and V_{oc}) can be successfully calculated by Equation (19) after two different operating points of the PV system under the same weather conditions are obtained.

In addition, according to Figures 6 and 7, it is obvious that the $I_{sc} - V_{oc}$ curve is also determined by D. The reason for this is that the parameters V (V_1 or V_2) and I (I_1 or I_2) are determined by D (D_1 or D_2). Therefore, to some extent, the unique solution under different D conditions reveals the feasibility, availability, and rationality of the equation solution.

5.1.3. Verification of Equation (20)

To test whether V_{bus} can be solved by Equation (20) or not, some simulation experiments were carried out and the simulation results are shown in Figure 8. Here, D_{m1}, D_{m2}, and D_{m3} represent the duty cycles at the MPP when V_{bus} is 12, 13, and 14 V, respectively.

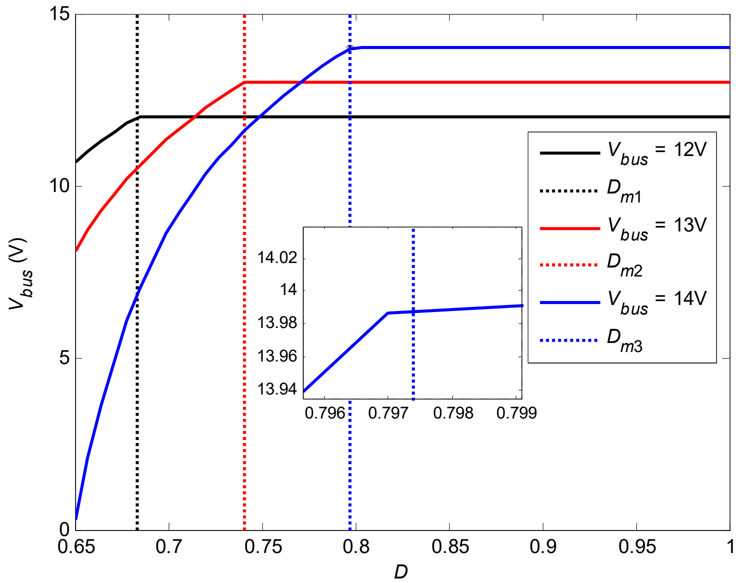

Figure 8. $V_{bus} - D$ curves for the verification of Equation (20).

Figure 8 shows that the real-time V_{bus} can be successfully solved by Equation (20), but the equation solution probably fails when D is less than D_m, corresponding to the given V_{bus}. In other words, the solution of V_{bus} is hardly accurate when $D < D_m$. Therefore, to make the solved V_{bus} accurate, the selected value of D must always be bigger than the corresponding D_m. In practical application, when V_{bus} is decreasing, an appropriate D can be used again and again while it must be continually updated under increasing V_{bus} conditions. Therefore, the simulation results shown in Figure 8 also verify that it is reasonable to set the default value of $D_{\max2}$ as 1 when V_{bus} is unknown or varying.

All in all, it is feasible and available to solve some main parameters of the ES-VWP method using Equations (19) and (20).

5.2. Accuracy of the Equation Solution

When the MPP of the PV system is tracked using the proposed ES-VWP method, the MPPT accuracy is determined by the accuracy of the equation solution of Equation (19). Therefore, some simulation experiments were carried out to analyze this issue. Here, Equations (23) and (24) can be used to estimate the accuracy of the equation solution when Equation (19) is used. Here, I_{sc} and V_{oc} represent the ideal values while I_{sc}^* and V_{oc}^* represent their solved values, respectively. E_{Isc} represents the error between I_{sc}^* and I_{sc}. Meanwhile, E_{Voc} represents the error between V_{oc}^* and V_{oc}. In addition, Table 1 shows the operating conditions of every simulation experiment. Here, D_0 represents the initial value of D in the simulation experiments:

$$E_{Isc} = I_{sc} - I_{sc}^* \quad (23)$$

$$E_{Voc} = V_{oc} - V_{oc}^{*} \tag{24}$$

Table 1. Operating conditions of the PV system corresponding to every simulation.

Operating Conditions	①	②	③	④	⑤	⑥
$S(\mathrm{W/m^2})$	variable	1000	variable	1000	variable	1000
$T(^{\circ}\mathrm{C})$	25	variable	25	variable	25	variable
D_0	0.91	0.91	variable	variable	0.95	0.96
ΔD	0.001	0.001	0.001	0.001	variable	variable
$V_{bus}(\mathrm{V})$	15	15	15	15	15	15

5.2.1. Accuracy under Varying Weather Conditions

The accuracy of I_{sc}^{*} and V_{oc}^{*} can be analyzed under varying irradiance (S) conditions (① in Table 1) and varying temperature (T) conditions (② in Table 1). On the one hand, under ① conditions, two simulations were conducted and the results are shown in Figures 9 and 10. Here, the $E_{Isc} - S$ curve is shown in Figure 9 and the $E_{Voc} - S$ curve is shown in Figure 10. On the other hand, two simulations were also carried out, and the $E_{Isc} - T$ and $E_{Voc} - T$ curves are shown in Figures 11 and 12, respectively, under the ② conditions.

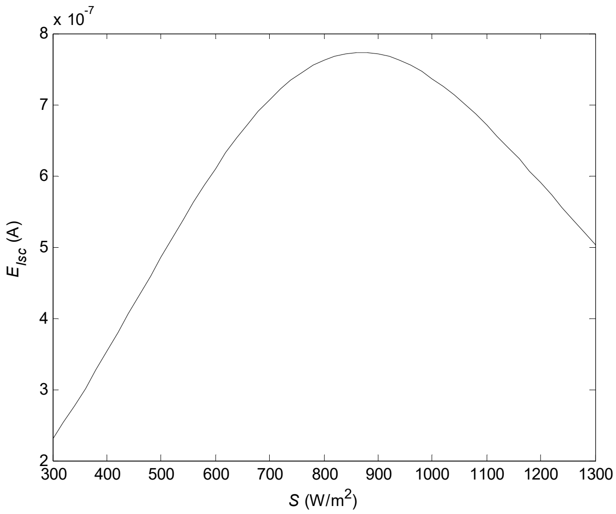

Figure 9. $E_{Isc} - S$ curve corresponding to ①.

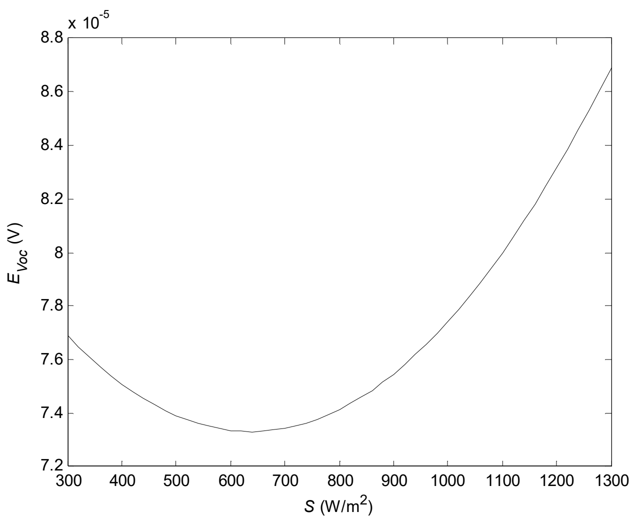

Figure 10. $E_{Voc} - S$ curve corresponding to ①.

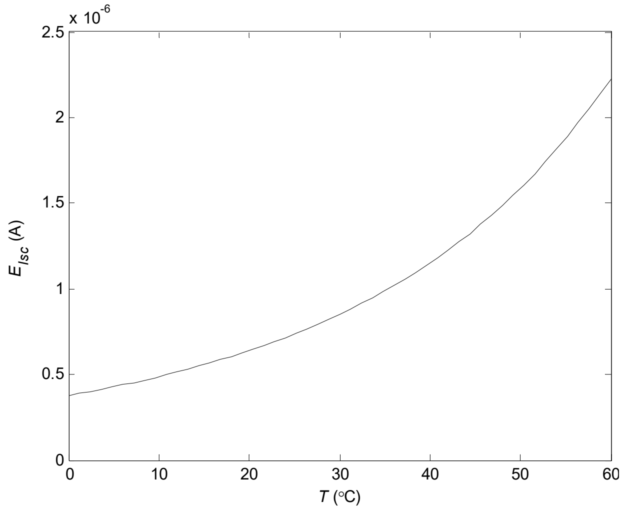

Figure 11. $E_{Isc} - T$ curve corresponding to ②.

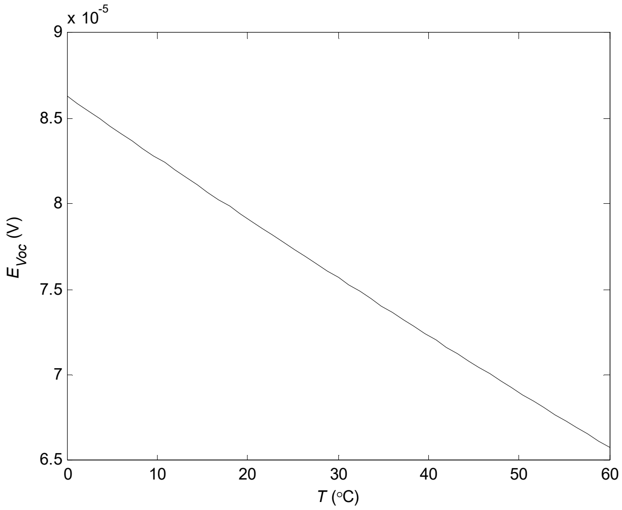

Figure 12. $E_{Voc} - T$ curve corresponding to ②.

Figure 9 shows that I_{sc}^* is approximately equal to I_{sc} and the error between them is less than 0.001 mA under varying S conditions. Meanwhile, Figure 10 shows that V_{oc}^* is approximately equal to V_{oc} and the error between them is less than 0.1 mV under varying S conditions. Figure 11 shows that the error between I_{sc}^* and I_{sc} is always less than 0.003 mA under varying T conditions. In addition, Figure 12 shows that the error between V_{oc}^* and V_{oc} is always less than 0.1 mV under varying T conditions.

Therefore, a conclusion can be drawn that the accuracy of I_{sc}^* and V_{oc}^* is very good under varying weather conditions.

5.2.2. Influence of the Initial Value D_0 on the Accuracy

Whether the accuracy of the equation solution is influenced by D_0 can be analyzed by two simulations under varying S conditions (③ in Table 1) and two simulations under varying T conditions (④ in Table 1). On the one hand, under ③ conditions, the simulation results are shown in Figures 13 and 14. Here, the $E_{Isc} - S$ curve is shown in Figure 13 and the $E_{Voc} - S$ curve is shown in Figure 14. On the other hand, under ④ conditions, the simulation results are shown by the $E_{Isc} - T$ curve in Figure 15 and the $E_{Voc} - T$ curve in Figure 16, respectively.

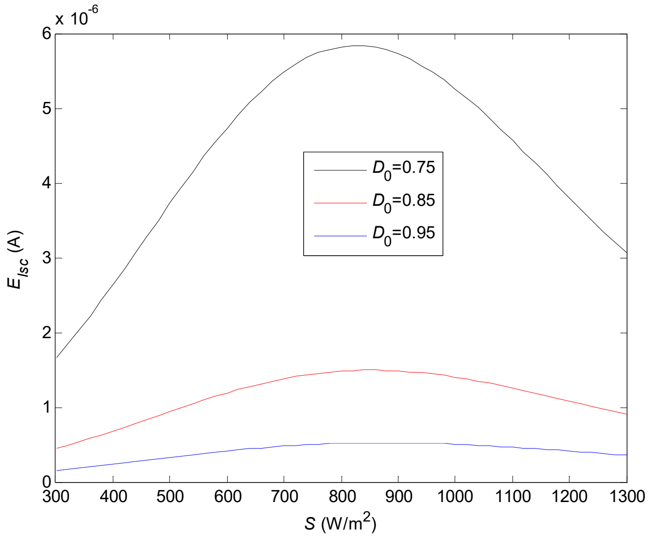

Figure 13. $E_{Isc} - S$ curve corresponding to ③.

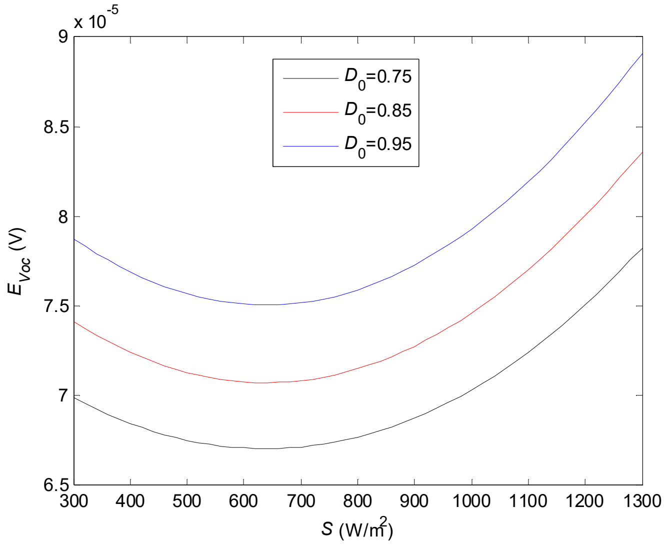

Figure 14. $E_{Voc} - S$ curve corresponding to ③.

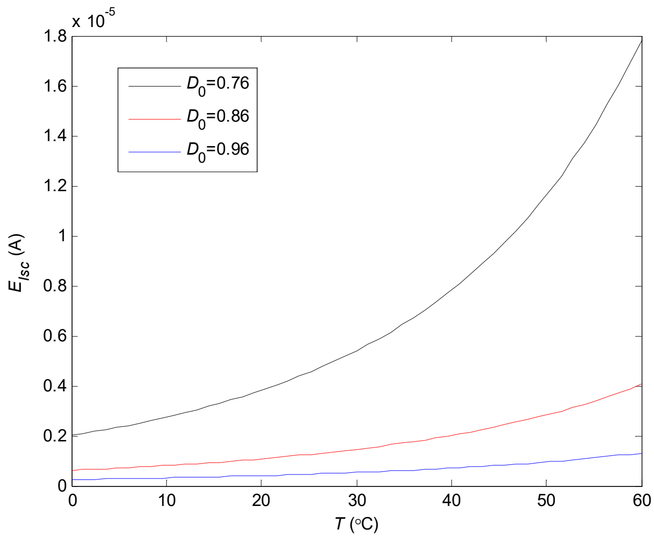

Figure 15. $E_{Isc} - T$ curve corresponding to ④.

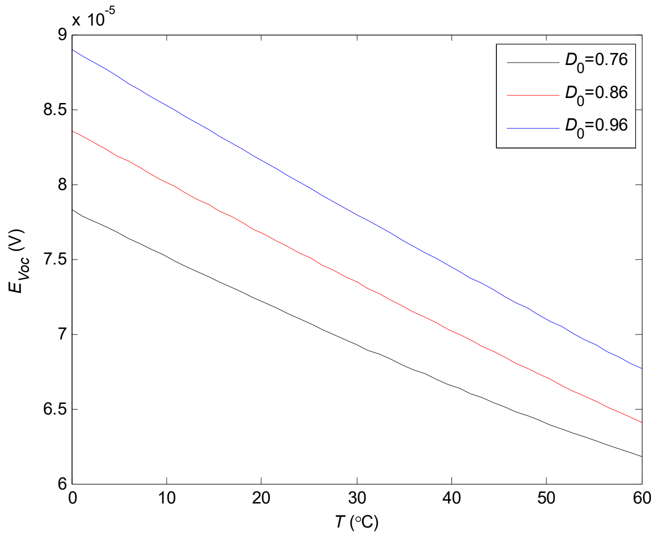

Figure 16. $E_{Voc} - T$ curve corresponding to ④.

Figure 13 shows that the error between I_{sc}^* and I_{sc} is less than 0.01 mA under varying S and different D_0 conditions. Figure 14 shows that the error between V_{oc}^* and V_{oc} is less than 0.1 mV under varying S and different D_0 conditions. Figure 15 shows that the error between I_{sc}^* and I_{sc} is less than 0.02 mA under varying T and different D_0 conditions. Figure 16 shows that the error between V_{oc}^* and V_{oc} is less than 0.1 mV under varying T and different D_0 conditions. In addition, according to Figures 13 and 15, it is obvious that the error between I_{sc}^* and I_{sc} increases with the decrease in D_0. In contrast, Figures 14 and 16 show that the error between V_{oc}^* and V_{oc} increases with the increase in D_0.

Therefore, a conclusion can be drawn that the accuracy of I_{sc}^* and V_{oc}^* is hardly influenced by the initial value D_0.

5.2.3. Influence of ΔD on the Accuracy

Whether the accuracy of the equation solution is influenced by ΔD can also be analyzed by two simulations under varying S conditions (⑤ in Table 1) and two simulations under varying T conditions (⑥ in Table 1). On the one hand, under ⑤ conditions, the simulation results are shown by the $E_{Isc} - S$ curve in Figure 17 and the $E_{Voc} - S$ curve in Figure 18, respectively. On the other hand, under ⑥ conditions, the simulation results are shown by the $E_{Isc} - T$ curve in Figure 19 and the $E_{Voc} - T$ curve in Figure 20, respectively.

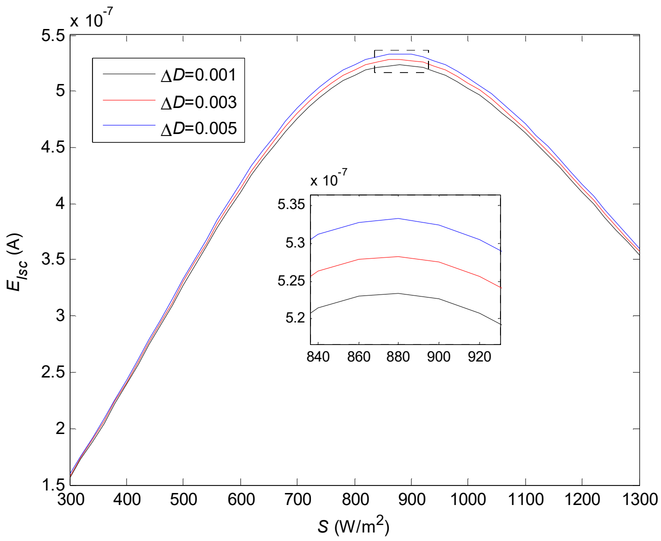

Figure 17. $E_{Isc} - S$ curve corresponding to ⑤.

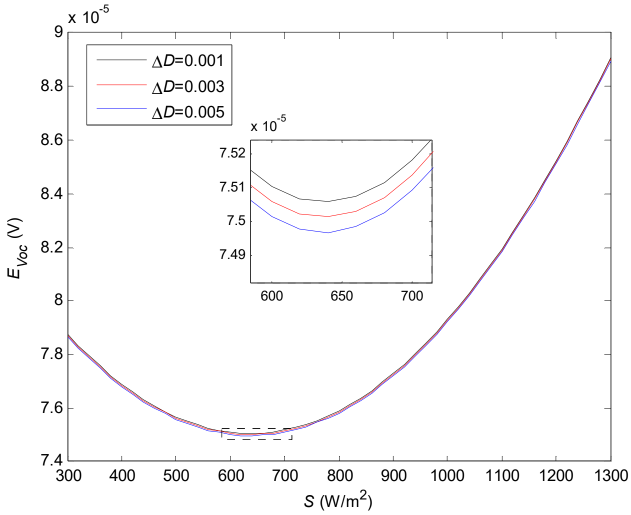

Figure 18. $E_{Voc} - S$ curve corresponding to ⑤.

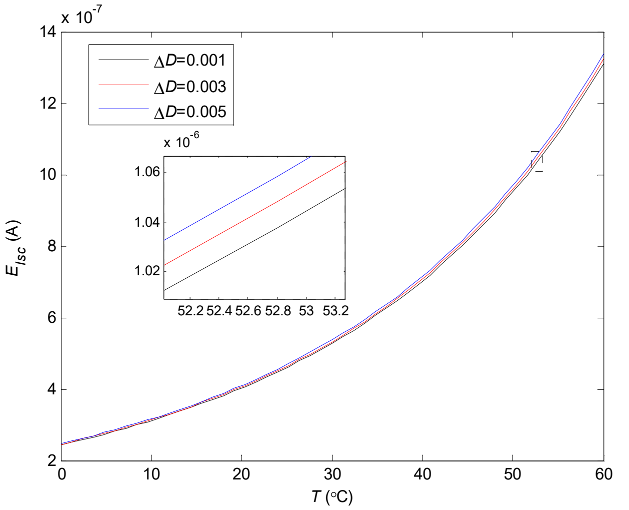

Figure 19. $E_{Isc} - T$ curve corresponding to ⑥.

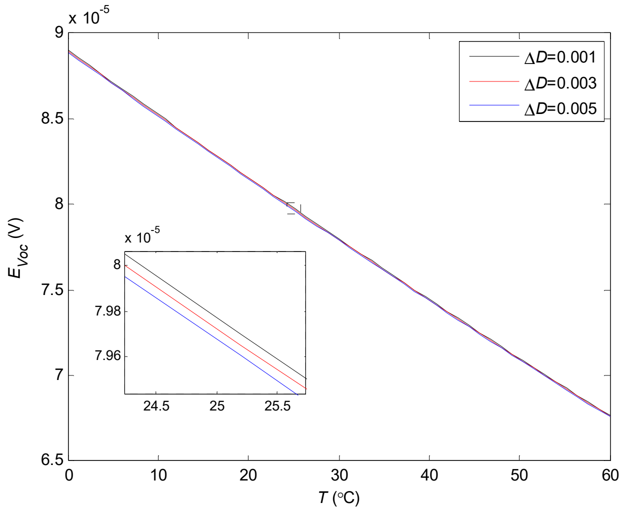

Figure 20. $E_{Voc} - T$ curve corresponding to ⑥.

Figure 17 shows that the error between I_{sc}^* and I_{sc} is less than 0.001 mA under varying S and different ΔD conditions. Figure 18 shows that the error between V_{oc}^* and V_{oc} is less than 0.1 mV under varying S and different ΔD conditions. Figure 19 shows that the error between I_{sc}^* and I_{sc} is less than 0.002 mA under varying T and different ΔD conditions. Figure 20 shows that the error between V_{oc}^* and V_{oc} is less than 0.1 mV under varying T and different ΔD conditions. In addition, according to Figures 17 and 19, it is obvious that the error between I_{sc}^* and I_{sc} slightly increases with the increase in ΔD. In contrast, Figures 18 and 20 show that the error between V_{oc}^* and V_{oc} slightly increases with the decrease in ΔD.

Therefore, a conclusion can be drawn that the accuracy of I_{sc}^* and V_{oc}^* is hardly influenced by the different ΔD.

All in all, the calculated values of I_{sc} and V_{oc} can be accurately obtained by the equation solution regardless of the varying S, T, D_0, or ΔD.

5.3. Feasibility and Availability of the Proposed Method

5.3.1. Analysis under Varying S Conditions

To analyze the feasibility and availability of the ES-VWP method, some simulations were carried out under 15 different S conditions when T, V_{bus}, D_0, and ΔD were set as 25 °C, 15 V, 0.8, and 0.001, respectively. The simulation results are shown in Table 2. Here, in Tables 2–6, I_{sc}^* and V_{oc}^* represent the solved values of I_{sc} and V_{oc}, respectively; V_1^*, V_2^*, I_1^*, and I_2^* represent the measured mean values of V_1, V_2, I_1, and I_2, respectively; $D_{\max}^*$ and $D_{\max 2}^*$ represent the calculated values of $D_{\max}$ and $D_{\max 2}$, respectively; $P_{o\max}^*$ and $P_{o\max 2}^*$ represent the output powers of PV subsystem 1 and PV subsystem 2, respectively; and D_m represents the ideal value of $D_{\max}$.

Table 2. Results under different irradiance conditions.

S (W/m^2)	V_1^*(V)	I_1^*(A)	V_2^*(V)	I_2^*(A)	V_{oc}^*(V)	I_{sc}^*(A)	$D_{\max}^*$	$D_{\max 2}^*$	$P_{o\max}^*$(W)	$P_{o\max 2}^*$(W)	D_m
300	17.8282	2.5233	17.8494	2.5203	21.9046	2.7570	0.8414	0.8404	44.9859	44.9855	0.8413
400	17.5772	3.3644	17.5777	3.3604	21.5716	3.6760	0.8544	0.8534	59.0694	59.0689	0.8543
500	17.3780	4.2055	17.3981	4.2006	21.3515	4.5950	0.8632	0.8622	73.0831	73.0825	0.8631
550	17.3237	4.6261	17.3438	4.6207	21.2849	5.0545	0.8659	0.8649	80.1406	80.1399	0.8658
600	17.2934	5.0466	17.3134	5.0407	21.2476	5.5140	0.8674	0.8664	87.2730	87.2723	0.8674
650	17.2871	5.4672	17.3071	5.4608	21.2398	5.9735	0.8677	0.8667	94.5113	94.5105	0.8677
700	17.3048	5.8877	17.3248	5.8809	21.2616	6.4330	0.8668	0.8658	101.8859	101.8850	0.8668
750	17.3466	6.3083	17.3666	6.3009	21.3129	6.8925	0.8647	0.8637	109.4266	109.4257	0.8647
800	17.4121	6.7288	17.4323	6.7209	21.3934	7.3520	0.8615	0.8605	117.1626	117.1616	0.8614
850	17.5016	7.1494	17.5216	7.1410	21.5028	7.8115	0.8571	0.8561	125.1220	125.1210	0.8571
900	17.6134	7.5699	17.6341	7.5610	21.6408	8.2710	0.8516	0.8506	133.3320	133.3309	0.8516
950	17.7485	7.9905	17.7695	7.9809	21.8067	8.7305	0.8451	0.8441	141.8182	141.8171	0.8451
1000	17.9057	8.4110	17.9271	8.4009	21.9999	9.1900	0.8377	0.8367	150.6052	150.6039	0.8377
1100	18.2846	9.2521	18.3069	9.2407	22.4654	10.1090	0.8204	0.8194	169.1709	169.1693	0.8203
1200	18.7445	10.0932	18.7680	10.0805	23.0304	11.0280	0.8002	0.7992	189.1922	189.1903	0.8002

Table 3. Results under different temperature conditions.

T (°C)	V_1^*(V)	I_1^*(A)	V_2^*(V)	I_2^*(A)	V_{oc}^*(V)	I_{sc}^*(A)	$D_{\max}^*$	$D_{\max 2}^*$	$P_{o\max}^*$(W)	$P_{o\max 2}^*$(W)	D_m
−20	20.2263	7.4648	20.2536	7.4546	24.8511	8.1561	0.7416	0.7406	150.9847	150.9830	0.7416
−10	19.7106	7.6750	19.7366	7.6649	24.2175	8.3859	0.7610	0.7600	151.2799	151.2783	0.7610
0	19.1949	7.8853	19.2195	7.8751	23.5839	8.6156	0.7815	0.7805	151.3582	151.3567	0.7814
5	18.9371	7.9905	18.9610	7.9803	23.2671	8.7305	0.7921	0.7911	151.3161	151.3146	0.7921
10	18.6793	8.0956	18.7025	8.0854	22.9503	8.8454	0.8030	0.8020	151.2197	151.2182	0.8030
15	18.4214	8.2007	18.4441	8.1906	22.6335	8.9602	0.8143	0.8133	151.0691	151.0677	0.8142
20	18.1636	8.3059	18.1856	8.2957	22.3167	9.0751	0.8258	0.8248	150.8643	150.8629	0.8258
25	17.9057	8.4110	17.9271	8.4009	21.9999	9.1900	0.8377	0.8367	150.6052	150.6039	0.8377
30	17.6479	8.5161	17.6687	8.5061	21.6831	9.3049	0.8500	0.8490	150.2920	150.2907	0.8499
35	17.3900	8.6213	17.4102	8.6112	21.3663	9.4197	0.8626	0.8616	149.9245	149.9232	0.8625
40	17.1322	8.7264	17.1518	8.7164	21.0495	9.5346	0.8755	0.8745	149.5027	149.5016	0.8755
45	16.8744	8.8316	16.8934	8.8216	20.7327	9.6495	0.8889	0.8879	149.0269	149.0257	0.8889
50	16.6165	8.9367	16.6349	8.9267	20.4159	9.7644	0.9027	0.9017	148.4967	148.4956	0.9027
55	16.3587	9.0418	16.3765	9.0319	20.0991	9.8792	0.9169	0.9159	147.9124	147.9113	0.9169
60	16.1008	9.1470	16.1181	9.1371	19.7823	9.9941	0.9316	0.9306	147.2738	147.2728	0.9316

Table 4. Results under different temperature conditions.

V_{bus} (V)	V_1^*(V)	I_1^*(A)	V_2^*(V)	I_2^*(A)	V_{oc}^*(V)	I_{sc}^*(A)	$D_{\max}^*$	$D_{\max2}^*$	$P_{o\max}^*$(W)	$P_{o\max2}^*$(W)	D_m
17	17.6628	6.6447	17.6812	6.6377	21.7015	7.2601	0.9625	0.9615	117.3641	117.3633	0.9624
16	17.6628	6.6447	17.6823	6.6373	21.7015	7.2601	0.9059	0.9049	117.3641	117.3632	0.9058
15	17.6628	6.6447	17.6836	6.6368	21.7015	7.2601	0.8492	0.8482	117.3641	117.3631	0.8492
14	17.6628	6.6447	17.6851	6.6362	21.7015	7.2601	0.7926	0.7916	117.3641	117.3629	0.7926
13	17.6628	6.6447	17.6869	6.6356	21.7015	7.2601	0.7360	0.7350	117.3641	117.3628	0.7360
12	17.6628	6.6447	17.6889	6.6348	21.7015	7.2601	0.6794	0.6784	117.3641	117.3625	0.6794
11	17.6628	6.6447	17.6912	6.6339	21.7015	7.2601	0.6228	0.6218	117.3641	117.3622	0.6228
10	17.6628	6.6447	17.6941	6.6328	21.7015	7.2601	0.5662	0.5652	117.3641	117.3618	0.5661

Table 5. Results corresponding to Figures 21 and 22.

Time Interval (s)	S(W/m^2)	D_m	$D_{\max}^*$	$D_{\max}^{\&}$	$D_{\max}^F$	$D_{\max}^V$	$P_{o\max}^*$ (W)	$P_{o\max2}^*$ (W)	$P_{o\max}^{\&}$ (W)	$P_{o\max}^F$ (W)	$P_{o\max}^V$ (W)	t_s^* (ms)	$t_s^{\&}$ (ms)	t_s^F (ms)	t_s^V (ms)
[0, 0.4]	406	0.6840	0.6840	0.6835	0.6834	0.6835	59.91	59.91	59.91	59.91	59.91	5.4	220	118	6
[0.4, 0.7]	1202	0.6398	0.6398	0.6400	0.6402	0.6403	189.61	189.61	189.61	189.61	189.61	5.8	75	49	6
[0.7, 1]	498	0.6904	0.6904	0.6890	0.6894	0.6895	72.80	72.80	72.80	72.80	72.80	6	84	54	6

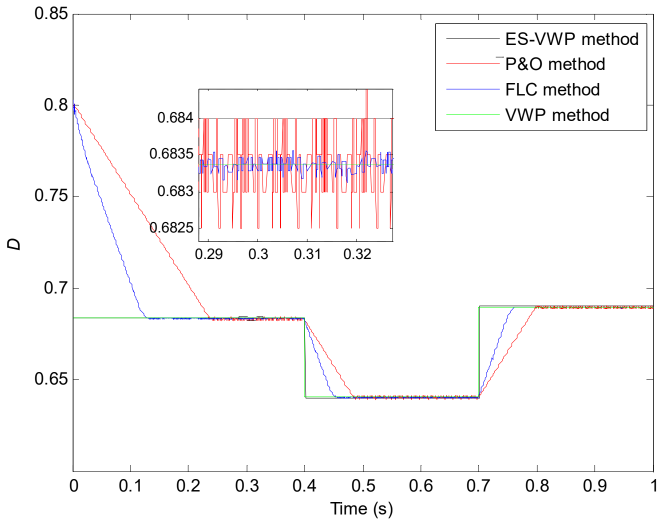

Figure 21. Simulation results of the duty cycles.

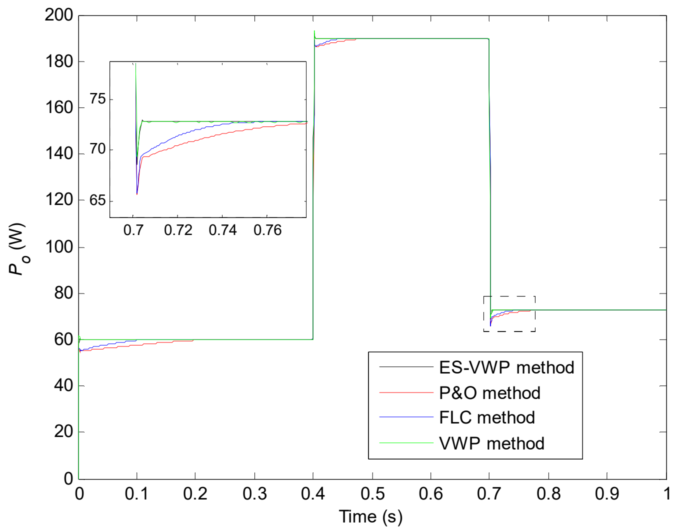

Figure 22. Simulation results of the output powers.

Table 6. Results corresponding to Figures 23 and 24.

Time Interval (s)	T (°C)	D_m	$D^*_{\max}$	$D^{\&}_{\max}$	$D^F_{\max}$	$D^V_{\max}$	$P^*_{o\max}$ (W)	$P^*_{o\max2}$ (W)	$P^{\&}_{o\max}$ (W)	$P^F_{o\max}$ (W)	$P^V_{o\max}$ (W)	t^*_s (ms)	$t^{\&}_s$ (ms)	t^F_s (ms)	t^V_s (ms)
[0, 0.4]	5	0.6337	0.6336	0.6336	0.6338	0.6336	151.32	151.31	151.32	151.32	151.32	5	330	148	6
[0.4, 0.7]	60	0.7453	0.7453	0.7455	0.7453	0.7453	147.28	147.27	147.28	147.27	147.28	6	210	110	6
[0.7, 1]	1.8	0.6282	0.6282	0.6280	0.6282	0.6282	151.35	151.34	151.35	151.35	151.35	5	225	121	5.5

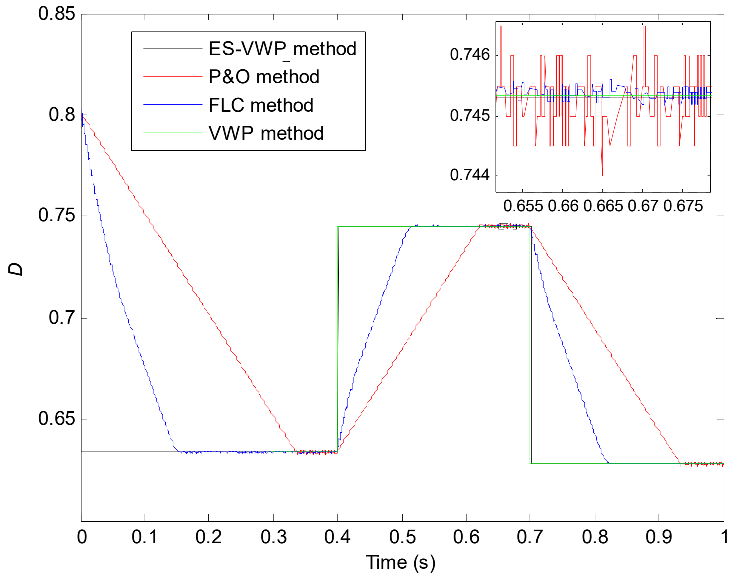

Figure 23. Simulation results of the duty cycles.

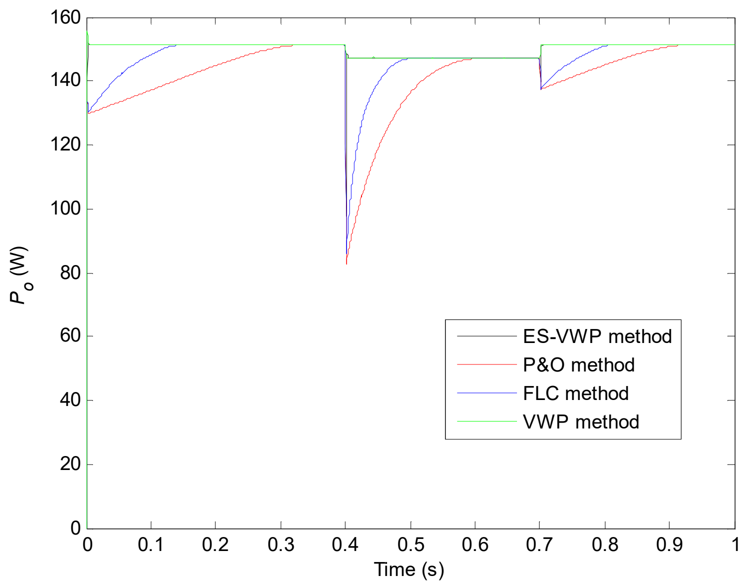

Figure 24. Simulation results of the output powers.

Table 2 shows that, on the one hand, $D^*_{\max}$ is almost equal to its corresponding D_m under different S conditions, which means that the ES-VWP method is feasible, available, and accurate. On the other hand, the error between $P^*_{o\max}$ and $P^*_{o\max2}$ is always less than 0.01 W, which means that PV subsystem 2 (shown in Figure 7) is operating around the MPP. Therefore, the ES-VWP method is available and feasible when S varies.

5.3.2. Analysis under Varying T Conditions

To test the feasibility and availability of the ES-VWP method, some simulations were carried out under 15 different T conditions when S, V_{bus}, D_0, and ΔD were set as 1000 W/m^2, 15 V, 0.8, and 0.001, respectively. Table 3 shows the results.

Table 3 shows that, firstly, $D^*_{\max}$ is almost equal to its corresponding D_m under different T conditions, which means that the ES-VWP method is feasible, available, and accurate. Secondly, the error between $P^*_{o\max}$ and $P^*_{o\max2}$ is always less than 0.01 W, which means that PV subsystem 2 (shown in Figure 7) is operating around the MPP. Therefore, the ES-VWP method is available and feasible when T varies.

5.3.3. Analysis under Varying V_{bus} Conditions

Under 8 different V_{bus} conditions, some simulations were carried out when S, T, D_0, and ΔD were set as 800 W/m^2, 20 °C, 0.8, and 0.001, respectively. Table 4 shows the simulation results.

Table 4 shows that, firstly, $D^*_{\max}$ is almost equal to its corresponding D_m under different V_{bus} conditions, which means that the ES-VWP method is feasible, available, and accurate. On the other hand, the error between $P^*_{o\max}$ and $P^*_{o\max2}$ is always less than 0.01 W, which means that PV subsystem 2 (shown in Figure 7) is operating around the MPP. In addition, when the DC bus voltage varies, V^*_1, I^*_1, V^*_{oc}, I^*_{sc}, and $P^*_{o\max}$ remain constant. Therefore, the ES-VWP method is available and feasible when V_{bus} varies.

All in all, the ES-VWP method is always feasible and available regardless of the varying S, T, or V_{bus}.

5.4. MPPT Performance Comparison

Some simulations were carried out to analyze the MPPT performance of the ES-VWP method. Here, D_0 and ΔD were selected as 0.8 and 0.001, respectively; V_{bus} was selected as 12 V in Sections 5.4.1, 5.4.2 and 5.4.4; S and T were selected as 600 W/m^2 and 25 °C, respectively, in Section 5.4.3. In the existing MPPT methods, the P&O method and FLC method are the representatives of the conventional MPPT methods and intelligent MPPT methods, respectively. Therefore, in this work, they are used for comparison with the ES-VWP method. Meanwhile, the VWP method in [8] is also used as the representative of the state-of-the-art method for comparison of the MPPT performance. Here, the step size and initiate value D_0 of the P&O method were set as 0.0005 and 0.8, respectively. In addition, the results of the P&O method and FLC method are the mean values in Tables 5 and 6 because of their oscillation.

5.4.1. Performance under Varying S Conditions

Under varying S and 25 °C conditions, four simulation experiments were carried out. The results are shown together in Figures 21 and 22. The duty cycle curves are compared in Figure 21 while the output power curves are compared in Figure 22. The data corresponding to Figures 21 and 22 are shown in Table 5. Here, $D^{\&}_{\max}$ and $P^{\&}_{o\max}$ represent $D_{\max}$ and $P_{o\max}$ of the P&O method, respectively; $D^F_{\max}$ and $P^F_{o\max}$ represent $D_{\max}$ and $P_{o\max}$ of the FLC method, respectively; $D^V_{\max}$ and $P^V_{o\max}$ represent $D_{\max}$ and $P_{o\max}$ of the selected VWP method, respectively; and t^*_s, $t^{\&}_s$, t^F_s, and t^V_s represent the settling times of the ES-VWP method, P&O method, FLC method, and VWP method, respectively.

Figures 21 and 22 and Table 5 clearly show that, firstly, for the MPPT speed, the ES-VWP method is almost same as the selected VWP method while it is far better than the other two methods. Secondly, the accuracy of the ES-VWP method is a little better than the other three methods. However, the output power of the ES-VWP method is the same as the other three methods. Meanwhile, the accuracy of the output power in the PV subsystem 2 is hardly influenced. Taking the measuring error into account, it is almost certain that these four MPPT methods have the same accuracy under varying S conditions. Thirdly, steady-state oscillation exists in the P&O method and FLC method. Therefore, the ES-VWP method and VWP method show a better steady-state performance.

5.4.2. Performance under Varying *T* Conditions

Under varying T and 1000 W/m^2 conditions, four simulation experiments were carried out. The results are shown together in Figures 23 and 24. The duty cycle curves are compared in Figure 23 while the output power curves are compared in Figure 24. The data corresponding to Figures 23 and 24 are shown in Table 6.

Figures 23 and 24 and Table 6 clearly show that, firstly, for the MPPT speed, the ES-VWP method is almost the same as the selected VWP method while it is far better than the other two methods. Secondly, the accuracy of the ES-VWP method is a little better than the other three methods. However, the output power of the ES-VWP method (including PV subsystem 2) is the same as the P&O method, FLC method, and VWP method. Taking the measuring error into account, it is almost certain that these four MPPT methods have the same accuracy under varying T conditions. Thirdly, the steady-state oscillation of the P&O method and FLC method shows a better steady-state performance of the ES-VWP method and VWP method.

5.4.3. Performance under Varying V_{bus} Conditions

Under varying V_{bus} conditions, four simulation experiments were carried out. The results are shown together in Figures 25 and 26. The duty cycle curves are compared in Figure 25 while the output power curves are compared in Figure 26. The data corresponding to Figures 25 and 26 are shown in Table 7.

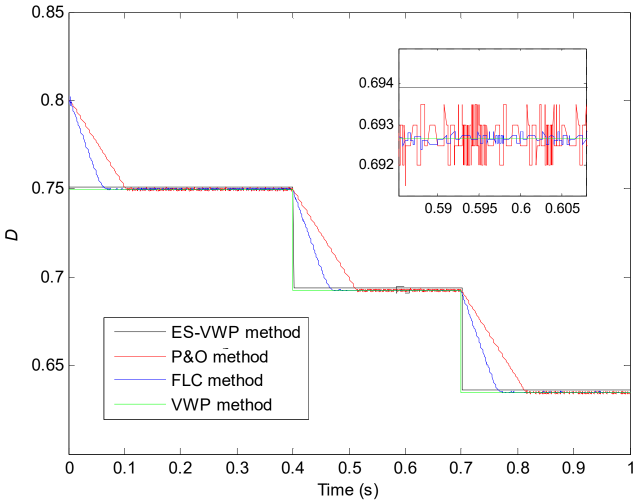

Figure 25. Simulation results of the duty cycles.

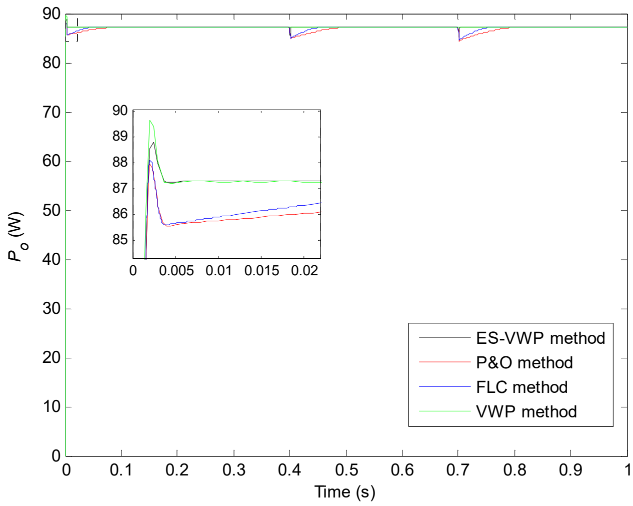

Figure 26. Simulation results of the output powers.

Table 7. Results corresponding to Figures 25 and 26.

Time Interval (s)	V_{bus} (V)	D_m	$D^*_{\max}$	$D^{\&}_{\max}$	$D^F_{\max}$	$D^V_{\max}$	$P^*_{o\max}$ (W)	$P^*_{o\max 2}$ (W)	$P^{\&}_{o\max}$ (W)	$P^F_{o\max}$ (W)	$P^V_{o\max}$ (W)	t^*_s (ms)	$t^{\&}_s$ (ms)	t^F_s (ms)	t^V_s (ms)
[0, 0.4]	13	0.7517	0.7511	0.7498	0.7499	0.7498	87.27	87.27	87.27	87.27	87.27	8	96	55	12
[0.4, 0.7]	12	0.6939	0.6939	0.6925	0.6927	0.6927	87.27	87.27	87.27	87.27	87.27	7	108	62	9
[0.7, 1]	11	0.6361	0.6360	0.6345	0.6350	0.6350	87.27	87.27	87.27	87.27	87.27	6.5	110	65	11

Figures 25 and 26 and Table 7 clearly show that, firstly, for the MPPT speed, the ES-VWP method is almost the same as the selected VWP method while they are far better than the other two methods. Secondly, the accuracy of the ES-VWP method is a little better than the other three methods. However, the output power of the ES-VWP method (including PV subsystem 2) is the same as the P&O method, FLC method, and VWP method. Taking the measuring error into account, it is almost certain that these four MPPT methods have the same accuracy under varying V_{bus} conditions. Thirdly, the steady-state oscillation of the P&O method and FLC method shows the better steady-state performance of the ES-VWP method and VWP method.

5.4.4. Performance under Arbitrary Conditions

By varying S and T arbitrarily, four simulation experiments were carried out. Figures 27 and 28 show the S curve and T curve, respectively. The results are shown together in Figures 29 and 30. The duty cycle curves are compared in Figure 29 while the output power curves are compared in Figure 30.

Figures 29 and 30 show that, firstly, the MPP can be successfully tracked by these four methods. However, two MPPT failures of the P&O method appear in time intervals [0, 0.2] and [0.4, 0.6], arising from the slow seeking speed. Secondly, the seeking speeds of the ES-VWP method and VWP method are always better than the other two methods. Thirdly, the output powers of the ES-VWP method and VWP method can be stabilized at the MPP. However, some oscillation appears in the other two methods. Fourthly, comparing the ES-VWP method with the VWP method, it is obvious that its MPPT speed is almost as good as the VWP method. In other words, without using irradiance and temperature sensors (or data), the good MPPT rapidity of the VWP method is successfully inherited by the ES-VWP method. Therefore, if the fact that the ES-VWP method successfully removed the irradiance and temperature sensors (or data) is considered, its whole performance is better than the VWP method.

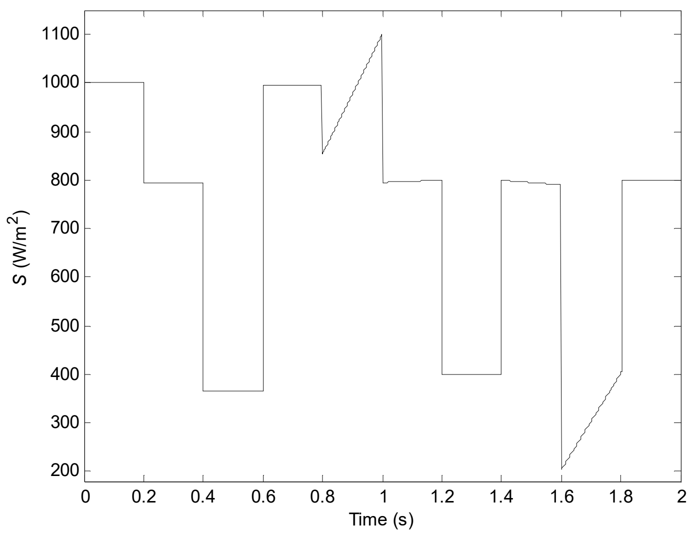

Figure 27. Varying S curve.

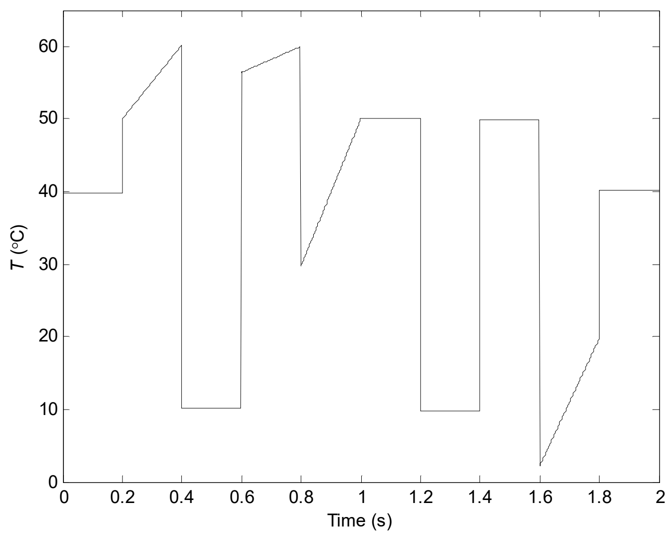

Figure 28. Varying *T* curve.

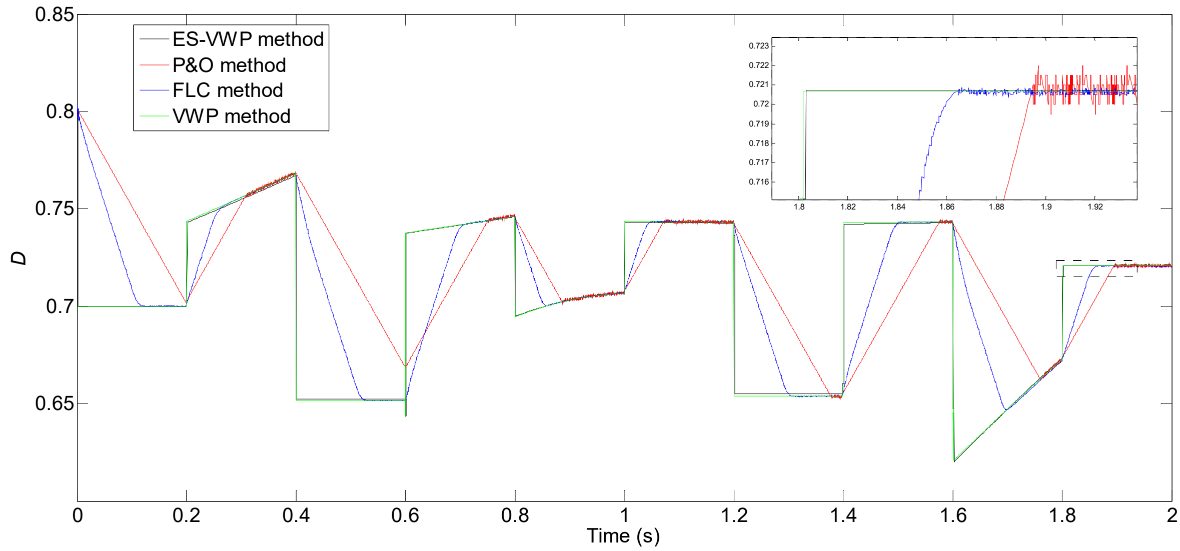

Figure 29. Simulation results of the duty cycles.

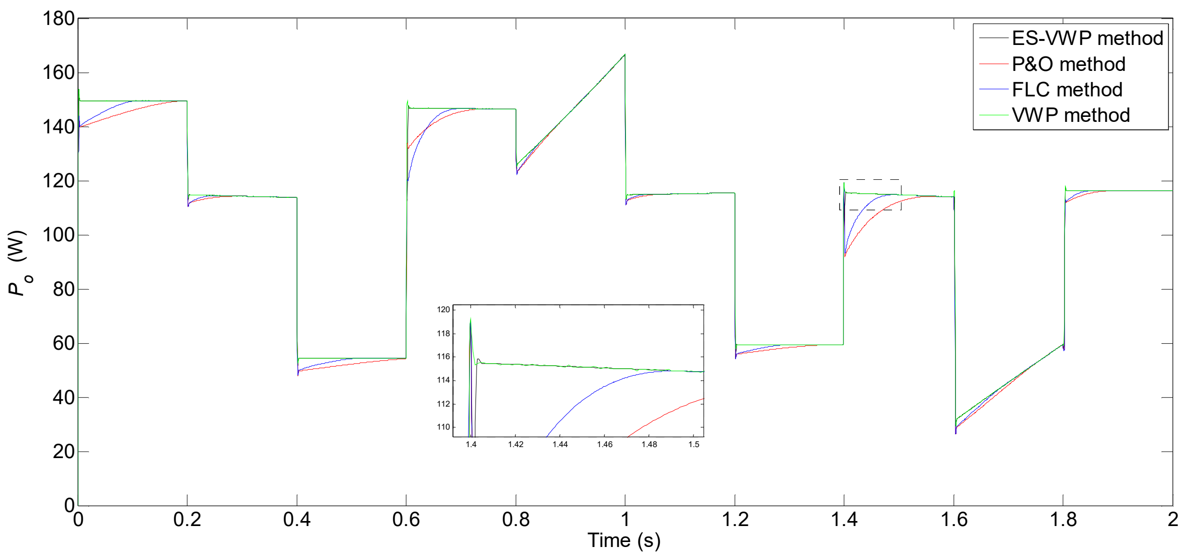

Figure 30. Simulation results of the output powers.

All in all, the ES-VWP method has better MPPT steady-state and transient-state performances than the conventional P&O method and FLC method. Meanwhile, in the case of no irradiance and temperature sensors (or data), its MPPT speed is almost as good as the VWP method.

6. Conclusions

In this paper, two equations of the PV system were combined as an equation set to directly solve the real-time V_{oc} and I_{sc}. Meanwhile, an equation solution method that can estimate the real-time value of the DC bus voltage was presented under unknown or varying bus voltage conditions. Based on them, an ES-VWP method, which is very different from all existing VWP methods and other MPPT methods, was proposed. In addition, an implementation method corresponding to the ES-VWP method was successfully designed using the PV system with a DC bus. Finally, many simulations verified the feasibility, availability, and workability of the proposed ES-VWP method. Meanwhile, these simulation results also showed better MPPT transient-state and steady-state performances than the conventional P&O method and FLC method. In this work, not only was the cost problem arising from irradiance and temperature sensors for all VWP methods solved but also good MPPT rapidity was achieved, which originates from the advantage of the VWP methods being inherited. Therefore, the proposed ES-VWP method can be regarded as an improved version of the VWP methods, especially from the point of view of the hardware cost and practical application.

Future work on the subject will be focused on applying the design idea and implementation method of this proposed MPPT strategy to other VWP methods, thereby reducing the hardware cost of the irradiance and temperature sensors.

Author Contributions: Conceptualization, S.L.; methodology, S.L.; software, S.L.; validation, S.L.; formal analysis, S.L.; investigation, S.L.; resources, S.L.; data curation, S.L.; writing—original draft preparation, S.L.; writing—review and editing, K.C. and Q.L.; visualization, S.L.; supervision, K.C. and Q.A.; project administration, S.L.; funding acquisition, S.L. All authors have read and agreed to the published version of the manuscript.

Funding: This work was supported by National Natural Science Foundation of China (No. 61963014).

Acknowledgments: The author would like to sincerely thank the editor and anonymous reviewers for their valuable comments and suggestions to improve the quality of the article.

Conflicts of Interest: The author declares no conflict of interest.

Nomenclature

MPP	maximum power point	D	duty cycle of the PWM signal of the DDC
MPPT	maximum power point tracking	S	solar irradiance
ES-VWP	VWP MPPT method based on equation solution	T	cell temperature
PV	photovoltaic	$D_{\max}$	D at the MPP
PWM	pulse-width modulation	I_{sc}	short circuit current of PV cell at STC
P&O	perturbation and observation	I_m	MPP current of PV cell at STC
INC	incremental conduction	V_{oc}	open circuit voltage of PV cell at STC
FLC	fuzzy logic control	V_m	MPP voltage of PV cell at STC
SSO	salp-swarm optimization	V	output voltage of PV cell
VWP	variable weather parameter	I	output current of PV cell
SCC	short-circuit current	V_o	output voltage of the DDC
I&T	irradiance and temperature	I_o	output current of the DDC
AC	alternating current	R_L	load or equivalent load resistance of PV system
DC	direct current	R_i	input resistance of the DDC
STC	standard test conditions	P_o	output power of PV system
DDC	DC/DC converter	V_{bus}	voltage of the DC bus

References

1. Danandeh, M.A.; Mousavi, G.S.M. Comparative and comprehensive review of maximum power point tracking methods for PV cells. *Renew. Sustain. Energy Rev.* **2018**, *82*, 2743–2767. [CrossRef]
2. Osmani, K.; Haddad, A.; Lemenand, T.; Castanier, B.; Ramadan, M. An investigation on maximum power extraction algorithms from PV systems with corresponding DC-DC converters. *Energy* **2021**, *224*, 120092. [CrossRef]
3. Zhang, X.; Gamage, D.; Wang, B.; Ukil, A. Hybrid maximum power point tracking method based on iterative learning control and perturb & observe method. *IEEE Trans. Sustain. Energy* **2021**, *12*, 659–670.
4. Danandeh, M.A.; Mousavi, G.S.M. A new architecture of INC-fuzzy hybrid method for tracking maximum power point in PV cells. *Sol. Energy* **2018**, *171*, 692–703. [CrossRef]
5. Li, X.; Wen, H.; Hu, Y.; Jiang, L. A novel beta parameter based fuzzy-logic controller for photovoltaic MPPT application. *Renew. Energy* **2019**, *130*, 416–427. [CrossRef]
6. Mirza, A.F.; Mansoor, M.; Ling, Q.; Yin, B.; Javed, M.Y. A Salp-Swarm Optimization based MPPT technique for harvesting maximum energy from PV systems under partial shading conditions. *Energy Convers. Manag.* **2020**, *209*, 112625. [CrossRef]
7. Li, S. A variable-weather-parameter MPPT control strategy based on MPPT constraint conditions of PV system with inverter. *Energy Convers. Manag.* **2019**, *197*, 111873. [CrossRef]
8. Li, S.; Ping, A.; Liu, Y.; Ma, X.; Li, C. A variable-weather-parameter MPPT method based on a defined characteristic resistance of photovoltaic cell. *Sol. Energy* **2020**, *199*, 673–684. [CrossRef]
9. Eltawil, M.A.; Zhao, Z. MPPT techniques for photovoltaic applications. *Renew. Sustain. Energy Rev.* **2013**, *25*, 793–813. [CrossRef]
10. Camilo, J.C.; Guedes, T.; Fernandes, D.A.; Melo, J.D.; Costa, F.F.; Sguarezi Filho, A.J. A maximum power point tracking for photovoltaic systems based on Monod equation. *Renew. Energy* **2019**, *130*, 428–438. [CrossRef]
11. Xu, Y.; Kong, X.; Zeng, Y.; Tao, S.; Xiao, X. A modeling method for photovoltaic cells using explicit equations and optimization algorithm. *Int. J. Electr. Power Energy Syst.* **2014**, *59*, 23–28. [CrossRef]
12. Li, S. A maximum power point tracking method with variable weather parameters based on input resistance for photovoltaic system. *Energy Convers. Manag.* **2015**, *106*, 290–299. [CrossRef]
13. Sher, H.A.; Murtaza, A.F.; Noman, A.; Addoweesh, K.E.; Al-Haddad, K.; Chiaberge, M. A new sensorless hybrid MPPT algorithm based on fractional short-circuit current measurement and P&O MPPT. *IEEE Trans. Sustain. Energy* **2015**, *6*, 1426–1434.
14. Li, S. A MPPT speed optimization strategy for photovoltaic system using VWP interval based on weather forecast. *Optik* **2019**, *192*, 162958. [CrossRef]
15. Goud, J.S.; Kalpana, R.; Singh, B.; Kumar, S. A Global Maximum Power Point Tracking Technique of Partially Shaded Photovoltaic Systems for Constant Voltage Applications. *IEEE Trans. Sustain. Energy* **2019**, *10*, 1950–1959. [CrossRef]
16. Valenciaga, F.; Inthamoussou, F.A. A novel PV-MPPT method based on a second order sliding mode gradient observer. *Energy Convers. Manag.* **2018**, *176*, 422–430. [CrossRef]
17. Tousi, S.R.; Moradi, M.H.; Basir, N.S.; Nemati, M. A function-based maximum power point tracking method for photovoltaic systems. *IEEE Trans. Power Electron.* **2016**, *31*, 2120–2128. [CrossRef]
18. Gerber, D.L.; Vossos, V.; Feng, W.; Marnay, C.; Nordman, B.; Brown, R. A simulation-based effificiency comparison of AC and DC power distribution networks in commercial buildings. *Appl. Energy* **2018**, *210*, 1167–1187. [CrossRef]
19. Renaudineau, H.; Donatantonio, F.; Fontchastagner, J.; Petrone, G.; Spagnuolo, G.; Martin, J.P.; Pierfederici, S. A PSO-based global MPPT technique for distributed PV power generation. *IEEE Trans. Ind. Electron.* **2015**, *62*, 1047–1058. [CrossRef]
20. Espinoza-Trejo, D.R.; Bárcenas-Bárcenas, E.; Campos-Delgado, D.U.; De Angelo, C.H. Voltage-oriented input-output linearization controller as maximum power point tracking technique for photovoltaic systems. *IEEE Trans. Ind. Electron.* **2015**, *62*, 3499–3507.
21. Tang, L.; Wang, X.; Xu, W.; Mu, C.; Zhao, B. Maximum power point tracking strategy for photovoltaic system based on fuzzy information diffusion under partial shading conditions. *Sol. Energy* **2021**, *220*, 523–534. [CrossRef]
22. Li, Q.; Zhao, S.; Wang, M.; Zou, Z.; Wang, B.; Chen, Q. An improved perturbation and observation maximum power point tracking algorithm based on a PV module four-parameter model for higher efficiency. *Appl. Energy* **2017**, *195*, 523–537. [CrossRef]
23. Gopi, R.R.; Sreejith, S. Converter topologies in photovoltaic applications—A review. *Renew. Sustain. Energy Rev.* **2018**, *94*, 1–14. [CrossRef]
24. Li, S.; Attou, A.; Yang, Y.; Geng, D. A maximum power point tracking control strategy with variable weather parameters for photovoltaic systems with DC bus. *Renew. Energy* **2015**, *74*, 478–488. [CrossRef]
25. Li, S.; Li, Q.; Qi, W.; Chen, K.; Ai, Q.; Ma, X. Two variable-weather-parameter models and linear equivalent models expressed by them for photovoltaic cell. *IEEE Access* **2020**, *8*, 184885–184900. [CrossRef]
26. Batarseh, M.G.; Za'ter, M.E. A MATLAB based comparative study between single and hybrid MPPT techniques for photovoltaic systems. *Int. J. Renew. Energy Res.* **2019**, *9*, 2023–2039.